land

MDPI

Article

Temporal Trajectory and Spatial Heterogeneity of Agricultural Land Change and Its Consequence for Ecosystem Service in the Heilongjiang Region of China over the Past Half-Century

Zherui Yin [1,2,3,†], Zexian Li [1,†], Lin Shi [1], Naiwen Zhang [1], Haiyan Zhang [2], Baofu Li [1] and Tao Pan [1,2,*]

[1] School of Geography and Tourism, Institute of Yellow River Ecology, Qufu Normal University, Rizhao 276826, China; yinzr@igsnrr.ac.cn (Z.Y.); lizexian1218@qfnu.edu.cn (Z.L.); shilin@qfnu.edu.cn (L.S.); znw051206@qfnu.edu.cn (N.Z.); libf@qfnu.edu.cn (B.L.)
[2] Key Laboratory of Land Surface Pattern and Simulation, Institute of Geographic Sciences and Natural Resources Research, Chinese Academy of Sciences, Beijing 100101, China; zhanghaiyan@igsnrr.ac.cn
[3] College of Geographical Science, Inner Mongolia Normal University, Hohhot 010022, China
* Correspondence: pantao@qfnu.edu.cn; Tel.: +86-1981-9509-889
† These authors contributed equally to this work.

Highlights

(1) Remote sensing satellite monitoring showed that the cover of cultivated land changed by +46,443.41 km^2 and a growth rate of agricultural reclamation of 10.27%.
(2) Only a 13.08% area increment in rain-fed farmland but high to 246.14% in paddy fields was observed, suggesting a drastic restructuring of the internal structure of cultivated.
(3) An important finding was that cultivated land change led to the three-quarters loss (i.e., 74.78%) of ecosystem services.
(4) Another discovery displayed that a large transformation of wetland into paddy fields brought about the huge loss of 847.85 $\times$ 10^8 yuan; by contrast, the process of extensive rain-fed farmland turning into paddy fields was only a small change of 3.38 $\times$ 10^8 yuan.

Abstract

Northeast China has undergone large-scale cultivation of agricultural land, accompanied by internal restructuring of paddy fields and rain-fed farmland. Such a land change process has an obvious impact on the ecosystem. However, the quantitative effects of long-term cultivation of land/internal structure on the eco-environment are still lacking in the Heilongjiang region, China's ecological barrier and grain base. To address this academic issue, the integrated method of land update technology, dynamic tracking, remote sensing classification, and improved ecosystem services were applied using satellite imagery and land products. Through satellite monitoring, the area of cultivated land changed from 127,221.71 to 173,665.12 km^2, with an increment of 46,443.41 km^2, expanding the central–northern parts and the eastern part over the past half-century. In different regions, all cities have undergone varying degrees of reclamation rate expansion ranging 0.71–29.62%. Regarding the structure, a quarter of the study area was covered by rain-fed farmland (25.29%), but the cultivation level of paddy fields (2.83%) was very low in 1970; after that, only a 13.08% increment in rain-fed farmland but a high increase of 246.14% in paddy fields was monitored from 1970 to 2020. Meanwhile, the source area of cultivated land was 59,271.48 km^2, with 60.41% from forest and grassland of the agricultural-forestry ecotone. Its destination area was 12,827.11 km^2, and 78.49% of the total was converted to construction land, forest, and grassland. From 1970 to 2020, the evaluated ecosystem service changed

Check for updates

Academic Editor: Shiliang Liu

Received: 20 February 2026
Revised: 18 March 2026
Accepted: 26 March 2026
Published: 29 March 2026

Copyright: © 2026 by the authors. Licensee MDPI, Basel, Switzerland. This article is an open access article distributed under the terms and conditions of the Creative Commons Attribution (CC BY) license.

from 15,575.87 to 12,495.72 $\times$ 10^8 yuan, showing a total loss of 3080.15 $\times$ 10^8 yuan and an annual turnover rate of 0.40%. An important calculation indicated that the expansion and shrinkage of cultivated land led to a 2303.46 $\times$ 10^8 yuan loss, which means that three-quarters (i.e., 74.78%) of ecosystem service loss was caused by cultivated land changes. Another key finding was that a large transformation of wetland into paddy fields brought about the huge loss of 847.85 $\times$ 10^8 yuan; by contrast, the process of extensive rain-fed farmland turning into paddy fields was only a small change of 3.38 $\times$ 10^8 yuan. Considering the ecological loss caused by cultivated land, the projects of returning farmland to forests and wetland protection should be implemented. This study provided important references for land system monitoring and environmental impact assessment in high-latitude regions around the world.

Keywords: long time series monitoring; structure of cultivated land; spatiotemporal evolution; ecosystem service; environmental effect; Heilongjiang province of Northeast China

1. Introduction

Cultivated land, as the most severely intervened land type by human activities [1], directly reshapes the ecological processes and service supply capacity of the Earth's surface on a global scale [2,3]. The Food and Agriculture Organization of the United Nations (FAO) and the Intergovernmental Panel on Climate Change (IPCC) have repeatedly reported that agricultural land expansion and its intensification were the important driving factors leading to biodiversity loss, weakened carbon sink function and disrupted hydrological cycles [4]. Under global warming and intensifying anthropogenic activities, the systematic monitoring of agricultural land systems and their associated environmental impacts has emerged as a critical academic priority in the pursuit of global ecological resilience and food security [4–7]. China, characterized by a large-scale population base and scarce agricultural land resources, has exhibited a distinctive evolution in its cultivated land patterns and associated environmental transformations, rendering it a representative case for studying the interplay between demographic pressure and land-use sustainability [8,9]. Since the 1980s, the geographic center of China's cultivated land has undergone a pronounced northward shift, with Northeast China emerging as a pivotal region for national ecological integrity and food security, owing to its fertile black soils, abundant hydrological resources, and climatic suitability for intensive agriculture [10,11]. The establishment of the cultivated land policy in 2006 institutionalized cultivated land as a non-negotiable ecological threshold at the national level. The launch of the Northeast Black Soil Protection Project in 2022 formalized core conservation objectives, including the enhancement of soil organic matter content and the restoration of native biodiversity [12,13]. The reform of these policies has not only demonstrated the scientific consensus on the importance of global sustainable land-use monitoring, but also established a human–land–environment system governance approach with Chinese characteristics, providing a key practical sample for cultivated land changes and environmental effects in high-latitude agricultural regions around the world.

Over the past half-century, land monitoring technology has evolved from ground surveys and aerial photography to an intelligent perception system centered on multi-source remote sensing imagery, providing a solid data foundation for quantifying spatiotemporal changes in cultivated land at global, continental, national, and regional scales [14]. Previously, due to technological limitations, although 1 km Moderate Resolution Imaging Spectroradiometer (MODIS) and 300 m European Space Agency (ESA) land products were relatively rough, they were still widely used in land monitoring [15]. In 1972, Landsat satel-

lite imagery was launched into space. Subsequently, scholars produced numerous land-use products relying on satellite imagery, such as Global Land Cover with 30 m resolution (GlobeLand30) and Global Land Cover with Fine Classification System at 30 m resolution (GLC_FCS 30) datasets [16]. The multi-period of both datasets effectively improved the monitoring level of cultivated land and its changes [17]. In the 2020s, the high-resolution series satellites and the aerial remote sensing systems achieved an important increase in accuracy, enabling multi-period aerial observations of 2 m or even sub-pixel farmland and accurately identifying the boundaries of farmland. Meanwhile, the integration of drone platforms and AI interpretation algorithms could achieve high accuracy in land classification, which far exceeded traditional manual inspections [18]. Although these technological advancements achieved a leap from macro-overview to micro-diagnosis in land monitoring, land-use vector products developed by the Chinese Academy of Sciences (CAS) using Landsat satellite imagery remained widely employed in China, which spanned a continuous temporal record from 1970 to the present and served as a foundational dataset for land dynamics and transitions at regional to national scales [19]. This means that the set of data had the advantage of long-term, continuous monitoring of cultivated land, with its refined classification system distinguishing between paddy fields and rain-fed farmland within the cultivated land. It facilitated the precise tracking of structural evolution in agricultural land use at high temporal resolution.

Ecosystem services constituted the foundational pillar of the Earth's life-support systems and human well-being, which covered four major categories of functions: supply, regulation, support, and culture [20]. The research of its ecosystem services commenced in the 1990s with the Costanza team's pioneering global assessment, which first systematically quantified the annual value of global ecosystem services at $33 trillion [21]. This study established an evaluation system based on equivalence factors and the market substitution method, accompanied by the integration of natural capital into economic valuation. Afterwards, Chinese scholars such as Xie Gaodi constructed the equivalent factor system applicable to the whole region of China based on Costanza and Chinese local ecological characteristics [22], which introduced the Chinese parameters such as biomass, precipitation, and soil conservation to correct regional differences. Then, after continuous revisions, this method improved the accuracy and practicality of the assessment [22]. Although it has been widely applied in ecosystem assessment in China and has achieved many rich academic achievements. Built-in ecosystems often set settlement environments as deserts, which could induce systematic underestimation of ecosystem service values and land-use dynamics in non-arid regions. Integration of remote sensing, GIS, and machine learning has enabled high-resolution mapping of settlement systems at regional to global scales, revealing the spatial mosaic and heterogeneity characteristics of the different ecological lands [23,24]. Through these remote sensing satellite classification technologies, a more detailed classification of ecological land within settlements could improve the accuracy of the ecosystem service equivalent factor method.

The expansion of cultivated land was not a homogeneous process and its impact on ecosystem services presented spatial heterogeneity. The transformation of wetlands and grasslands to agricultural use substantially diminished regional water conservation capacity and groundwater recharge dynamics [25]. The conversion of farmland towards forest land not only caused carbon sequestration losses, but also increased the risk of soil erosion and fragmentation of biological habitats. Considering the complexity of the impact of farmland evolution on ecosystems, this issue continued to be a focus of academic research. In Northeast China, land changes were mainly characterized by increased land cultivation and the sharply decreasing areas of natural ecosystems [26], causing the environmental issues of reduced soil organic matter and the accelerated soil erosion [27]. Therefore, Northeast

China continues to be a hot area for farmland and environmental research. However, the impact of long-term cultivated land evolution on ecosystem services is still lacking in this region. Therefore, the objective of this study is below: (1) to elucidate the contemporary status and spatiotemporal evolution patterns of cultivated land reclamation across the entire region and within each city, while simultaneously contrasting the evolved trajectories of paddy fields and rain-fed farmland between 1970 and 2020; (2) to track the sources and destinations of cultivated land and its internal structural changes, and capture the most important driving type of land system change; and (3) to assess the evolutionary trends of ecosystems and assess the impact of long-term cultivated land changes and its internal structure on ecosystem services, especially the shifting contributions of land transitions from paddy fields/rain-fed farmland to diverse forest types, grassland cover gradients and wetland extents. This study could offer actionable insights for optimizing remote sensing satellite applications, enhancing systematic land monitoring, refining agricultural production strategies, mitigating soil erosion, and advancing biodiversity conservation research in the context of land-use change.

2. Materials and Methods

2.1. Study Area

Heilongjiang region is the northernmost and highest-latitude region of China [28], with a location spanning from 121°11′ E to 135°05′ E and from 43°26′ N to 53°33′ N (Figure 1). It spans 14 longitudes from east to west and 10 latitudes from north to south. This region faces Russia across the river in the northeast, is adjacent to Inner Mongolia in the west, and is bordered by Jilin region in the south. Heilongjiang region is the core node of the Northeast Asia International Corridor and a national ecological security barrier. The region features elevated topography in the northwest, north, and southeast, with a pronounced lowland corridor stretching northeast to southwest, dominated by mountains (300–1000 m, 58%), plateaus (200–350 m, 14%), and plains (50–200 m, 28%). Heilongjiang region is located within a cold temperate to temperate continental monsoon zone, transitioning from temperate in the south to cold temperate in the north, and from humid zone in the east to semi-humid and semi-arid zones in the west. Seasonal patterns include dry, chilly springs; warm, wet summers contributing 60% of the annual 400–650 mm rainfall; early frost autumns; and long, frigid winters. The annual mean temperature is 3.9 °C, with 2300–3000 h of sunshine and a frost-free period of 100–160 days. A dense hydrological network includes the Heilongjiang, Wusuli, Songhua, and Suifen rivers, comprising 2881 drainage channels (>50 km^2) totaling 92,100 km in length [29]. The region's rich, high-organic matter soils support the extensive agricultural land expansion.

2.2. Data Sources

This research employed multifaceted data with vector-based land-use datasets from the CAS. Compared with raster data, the area statistics of vector data may be more accurate. We aimed to extend the temporal coverage of land research as much as possible to provide long monitoring and mapping. According to the needs of the research period, each interval was set to 10 years, and the land data in the years of 1970, 1980, 1990, 2000, and 2015 were first collected. For land in 1970, the land-use map was jointly conducted by local agricultural departments, geological teams, and research institutions. Human resources were organized at the county level to conduct field surveys of land types, with the plot as the survey unit. The cartographers simultaneously used the manned aircraft equipped with optical cameras to conduct low-altitude aerial photography, obtaining black-and-white aerial photographs at scales of 1:50,000 to 1:100,000 as base maps for mapping. These images underwent geometric correction and mosaicking to form continuous regional image

maps. Then, the 1970 land-use map was produced and aligned with subsequent data from 1980, 1990, 2000, 2010, and 2015 to form a comparable series. In these vector data from 1970 to 2015, the dataset contained six first-level categories (i.e., cultivated land, forest, grassland, water, construction land, and unutilized land), which were further divided into 25 s-level categories.

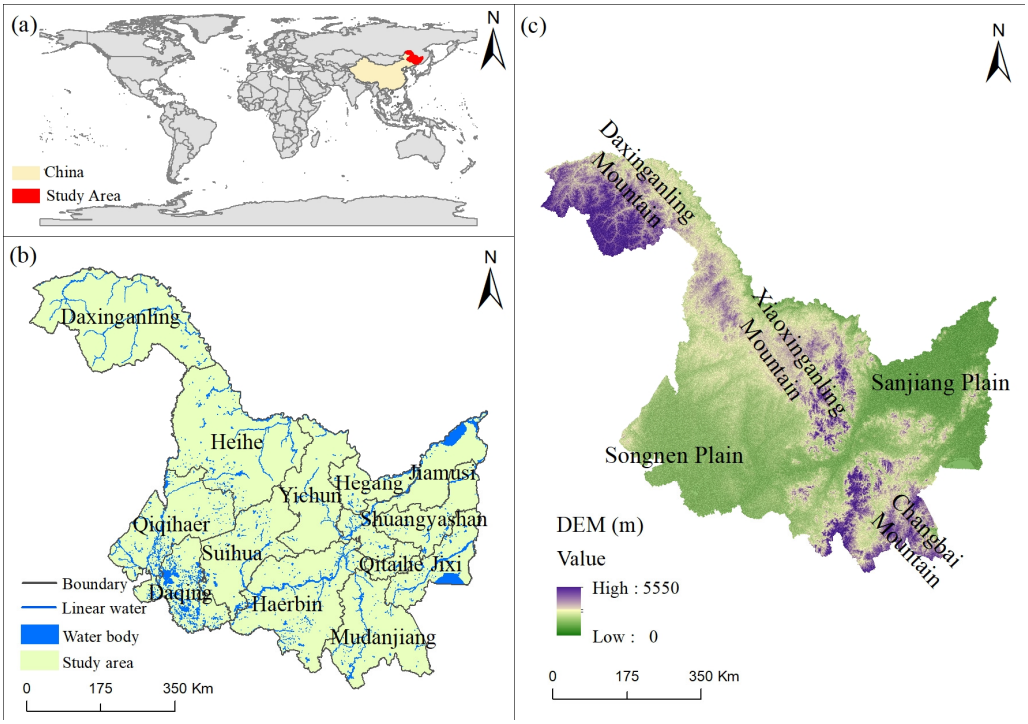

Figure 1. Administrative regions and Digital Elevation Model (DEM) of study area. Note: (**a**) Global location (i.e., red color), and (**b**,**c**) are the administrative division at the city-scale and the digital elevation map.

Regarding the selection of specific satellite imagery for land data production, based on the need to update land data for 2020 in this study, we reviewed the literature and found that data produced by the CAS were primarily derived from Landsat images [19]. To maintain comparability and consistency in classification systems with the previously generated land data from 1970 to 2010, this study also adopted Landsat series satellite images for the 2020 land update. And for the verified images, the validation of land data often used high-resolution images [19]. A Google image of 0.5 m was chosen due to its high-resolution and good accessibility. Landsat and Google images were used in this study. Landsat images adopted a sun-synchronous near polar orbit. They were downloaded from the data-sharing platform (website: https://www.gscloud.cn/ (accessed on 13 May 2025)). Each image's bands were downloaded because they were packaged in a compressed format containing all bands. During this process, we filtered the images with cloud cover, bad pixels, and poor quality. The centralized download time for images was from June to September, as the land surface features were relatively easy to identify during this period, with a total number of 216 scenes. The high-resolution Google imagery has also been downloaded from the http://91wemap.com/ (accessed on 13 May 2025) website. Other data, such as administrative divisions, digital elevation, rivers, etc., were sourced from the resource platform (website: https://www.resdc.cn/DOI/DOI.aspx?DOIID=54 (accessed on 13 May 2025)). And the socio-economic development and various statistical data were sourced from the CNKI academic-sharing platform (website: https://kns.cnki.net/res/cyfd (accessed

on 13 May 2025)) and the government statistics official website: https://tjj.hlj.gov.cn/ (accessed on 13 May 2025).

2.3. Technical Process

To meet the requirements of the study, a temporal interval of ten years was established to facilitate equidistant monitoring of land change and its environmental impacts, namely the 10-year intervals from 1970 to 2020. The land-use maps in the period of 1970–2015 were collected. All land-use maps were manually checked for data quality such as topology detection. Then, to obtain the 2020 land-use map, remote sensing satellite images were downloaded and further preprocessed through atmospheric correction, radiometric calibration, unified projection and coordinates. By combining land maps and remote sensing images, the 2020 land-use map was produced utilizing land map updating technology. Stratified random sampling scheme on ArcGIS 10.7 executed the accuracy evaluation. After 50 years of land data were complete, space extraction technology was applied to screen cultivated land and internal structural layers. Mathematical statistical methods were used to conduct the analysis of cultivated land reclamation rate. And land dynamic tracking technology further explored the sources and destinations of changes in cultivated land and internal structure. After that, to reveal ecosystem effects, the ecosystem service model was improved from the land system perspective. In this, matching the different land classification systems was first executed using the one-to-one land type approach. The internal classification of settlement ecology was conducted using the technologies of minimum noise fraction technique (MNF), vegetation-bare soil-impermeable surface area selection model (V-I-S), the fully constrained least squares spectral unmixing model (FCLS), and decision tree classification. The result of the proportional weights for subcategories of settlement ecosystem such as impermeable surface area (ISA), forest, grassland, and bare soil (BS) was added to the equal factor model to improve the simulation accuracy of ecosystem services. Finally, the ecological values for the different types of lands and the calculation of ecosystem services were calculated, and the ecological service effects of cultivated land evolution were investigated through spatial analysis techniques and mathematical statistical schemes on ENVI 5.6 and OriginPro 2024b. The detailed technical process is displayed below (Figure 2).

2.4. Methods

2.4.1. Land Map Updating Technology

Regarding the absence of the land-use vector data of 2020, we used the land2015 data and 2020 Landsat images to obtain it. To maintain comparability and consistency in land data production, this study continued to employ a human–computer interactive digital technique, which aligned with the methodology adopted by the CAS for generating such land data in 1970, 1980, 1990, 2000, 2010, and 2015 [19]. Firstly, for establishing an initial field for land2020 in the attribute table of land2015, the 2015 land map with vector format was added to a professional software-processing platform (i.e., ArcGIS 10.7). We added a column attribute named 'land2020' in the attribute table and used a field calculator function to make its land classification system value equal to that of 'land2015'. According to the calculated results, the land classification system value for land2015 and land2020 in the attribute table were exact the same. Secondly, the bands of green, red and near-infrared from Landsat satellite were integrated to obtain the false-color composite images. These 2020 images were added to professional software platforms as underlying data for land renewal maps, and the 2015 land data was placed in the upper layer of these images. Thirdly, land map updating technology was applied to update land data. During this process, human–computer interactive updating of land maps became the main

approach. The color, texture, shape, size, and surrounding features of land objects in remote sensing images often became key factors in determining the type of land in land2020. By continuously flashing and comparing the 2020 attribute table and 2020 images, the land classification system code table (i.e., the 2020 attribute table) was constantly being updated using the professional knowledge in remote sensing and geology. Finally, all value updates in the land2020 column were made, and the land2020 data was obtained.

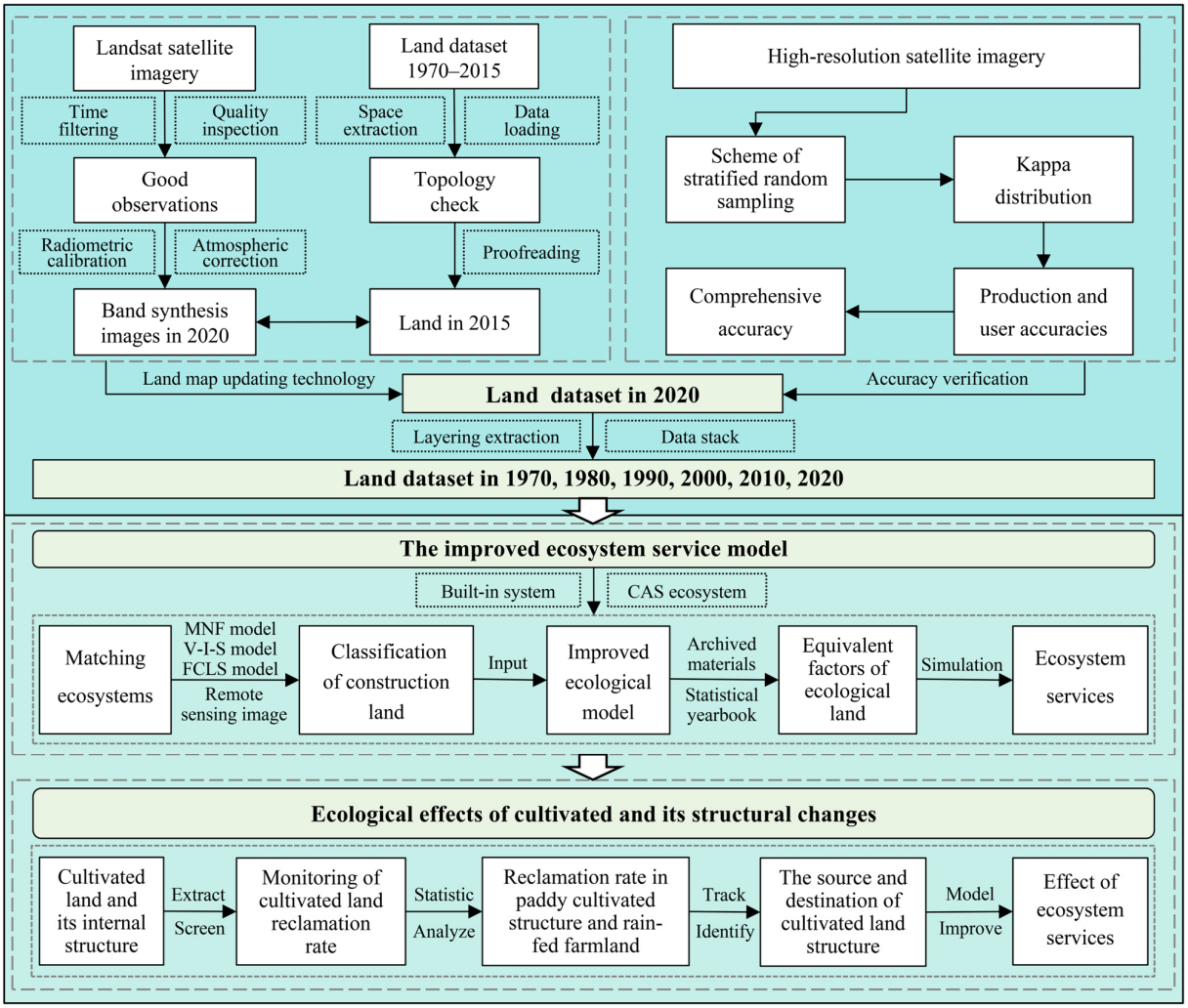

Figure 2. The technical process of this study.

The accuracy verification of the 2020 land-use map was launched accordingly. According to the land-use classification system, we randomly sampled each encoded layer, and the total number of sampling points for all layers was 500. These sampling points were added to the upper layer of high-resolution satellite imagery, and the true-false attributes of the sampling point land class were then identified. The correct number of samples, production and user accuracy, Kappa distribution, etc., were statistically analyzed. Comprehensive accuracy was 91.26%. Then, the land data in 1970, 1980, 1990, 2000, 2010 and 2020 was used for subsequent statistics, calculations, and analysis.

2.4.2. Dynamic Tracking Technology

Land dynamic tracking technology, as a core quantitative method for land-use dynamic monitoring, displayed the advantage in systematically, precisely, and traceably representing land category transition relationships. The method constructed a two-dimensional matrix with rows representing the initial time phase and columns representing the terminal

time phase, in which it solidified the area/component transition relationships among different land types in numerical form, transforming the originally ambiguous spatial change process into a computable, comparable, and predictable mathematical structure. Its characteristic was that it could track the source and destination of land types, accurately capturing their multi-period and continuous change trajectories. This study captured the evolutionary processes and trajectories of cultivated land from 1970 to 2020 and elucidated their relationships with various land-use types. Consequently, this method was employed in the presented study. The theory map of this method is displayed below (Figure 3).

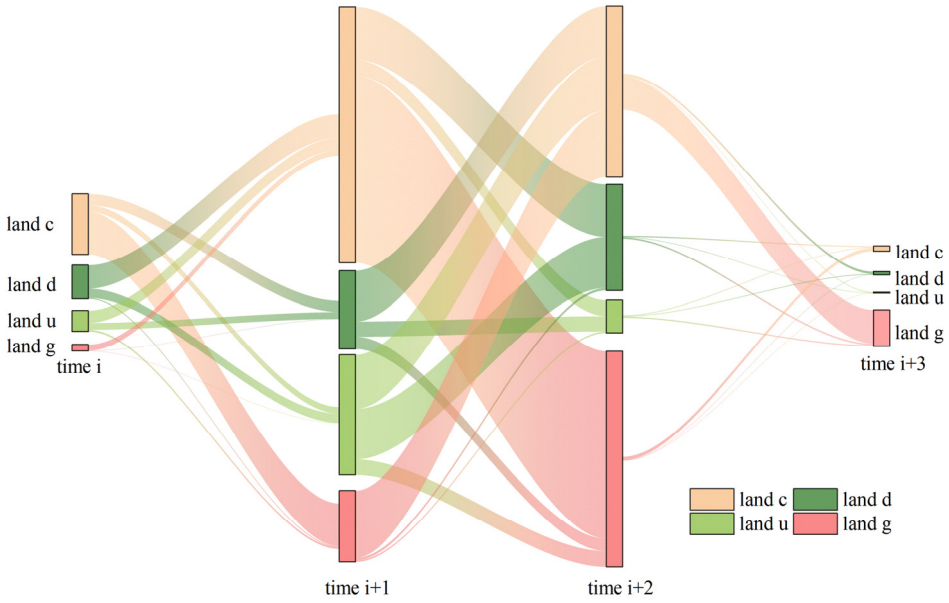

Figure 3. Theory map of land dynamic tracking technology. Note: The temporal stages are denoted by the indices i, i + 1, i + 2, and i + 3, progressing sequentially from earlier to later time points; the land types are represented by the labels land c, land d, land u, and land g.

2.4.3. The Improvement of Ecosystem Service Model from the Land System Perspective

Based on Costanza's global framework for ecosystem service valuation [21], the Chinese scholar Xie constructed the Chinese land ecosystem service equivalent factor model in 2003, in which this model established, for the first time, a standardized assessment system grounded in China's land-use types and was subsequently optimized in 2015 [22]. The model established one unit of farmland grain production value per unit area as one equivalent, with other ecosystem services scaled proportionally according to their relative contributions to achieve monetary comparability across different service types. It required land-use data and an equivalent factor table, and was particularly suitable for regional, large-scale, and long-term evaluations. This model has become the mainstream methodology for ecosystem services assessment, ecological compensation and the compilation of natural resource balance sheets in China. The study area, spanning over 45×10^4 km^2 and covering a long-term temporal sequence of 50 years, aligned precisely with the model's suitability characteristics. On this basis, we further optimized the localized parameters of settlement ecosystem services through remote sensing and field surveys, thereby enhancing the regional accuracy of model estimations.

In this study, the method was implemented in four steps. The ecological land systems between the model and the CAS should be firstly matched. Then, the proportions of internal land types of construction land were determined and used to improve the land ecosystem parameters. After that, the determination and value of the equivalent factor

of ecological service was calculated. Finally, the measurement of ecosystem services was executed. The specific method was displayed.

Matching the Different Land Classification Systems

There were many simulation models for ecosystem services, and in China the equivalent factor method developed by Xie was widely used in Chinese academia due to its adoption of localized parameters and universality [22]. In this model, there was a built-in land classification system, which contained the first-level land categories and the secondary land categories. By comparing the land classification system built-in the model with the CAS land classification system used in this study, we found the first-level land categories were the same in both land classification systems. By creating a one-to-one relationship in first-level land categories, the secondary land categories become connectable across both classification systems, such as rice field→rice field, upland crop→upland crop/rain-fed farmland, river system→reservoirs, ponds, rivers, and lakes, etc. Through such a link between the first-level and the second-level land categories, the one-to-one land type matching relationship from the simulated built-in land classification system in the model to the CAS land classification system was realized. This matching provided a foundation for the subsequent calculation of ecological factors and ecosystem services.

Internal Classification of Construction Land Based on the Surveys and the Remote Sensing Satellite Imagery

From a land perspective, the land classification system of the ecosystem service equivalent factor method that was widely used in China may have potential shortcomings, such as this model's setting of the ecological services of settlement systems as deserts. As is well known, although settlement spaces, such as cities and rural areas, contained a large number of roads, squares, roofs of houses, other cement, ceramic tiles, and steel structures similar to BS, they also contained road green spaces, community green spaces, lawns, forest belts, etc., to beautify the settlement landscape. Setting the settlement ecosystem as BS in the original equivalent factor method may not be appropriate. Especially, land types with high ecological services such as road green belts, block green spaces, parks, lawns, and forest belts within construction land may provide important service functions. Based on surveys and high-resolution satellites, this study classified the lands within the construction land to more land types, to improve the assessment in this model.

For the internal classification of construction land, the land types were first determined. The cement, asphalt, and tile areas of roads, roofs, and squares formed the regions where rainwater did not penetrate, which were considered as the ISAs. On the contrary, the regions where rainwater penetrated were divided into two types: one was the region with bare surface (i.e., BS), and the other was the region with vegetation (i.e., forest and grassland). The water within the construction land was ignored due to almost non-existent on-site investigations.

After determining the land type within the construction land, the satellite imagery and remote sensing classification techniques were implemented. MNF transformations decomposed the spectral space of multispectral imagery and concentrated the discriminative spectral signatures of land surface materials into the first three bands. Vegetation-bare soil-impermeable surface area selection model (V-I-S) further obtained the pure endmembers of vegetation coverage (VC), low-albedo objects (LAO), BS, and high-albedo objects (HAO). Endmembers of these four objects were then inputted into the FCLS model to generate density data (i.e., 0.01–100.00%) of VC, HAO, LAO, and BS. In this, the fully constrained least squares spectral unmixing model (FCLS) was a standard spectral unmixing algorithm whose core objective was to minimize the reconstruction error between the observed and linearly estimated spectral signatures under physical constraints. The model formulated

abundance estimation as a constrained quadratic optimization problem, ensuring the solution lied geometrically within the unit simplex, thereby guaranteeing physically meaningful results, namely, each pixel was composed of a linear mixture of pure material/endmember in non-negative proportions that sum to unity. It eliminated unrealistic components such as negative abundance or violation of the sum-to-one constraint. Its distinguishing feature was the strict enforcement of endmember abundances within the interval [0, 1], which significantly enhanced the fidelity of mixed pixel decomposition. Afterwards, a decision tree classifier was employed to delineate spatial land extents of ISA, forest, grassland, and BS by leveraging spectral density metrics and the normalized difference vegetation index (NDVI) as discriminative features. Finally, the boundaries of construction land were used to clip these data to obtain the different land classification area within the construction/delimited zone, and the corresponding proportion was calculated and further input into the land classification system to solve the problem of localizing construction land parameters.

Determination of Equivalent Factor Indicators

The formulation of an equivalence factor table has historically been anchored in ecological classifications, wherein the model integrated a proprietary classification hierarchy populated with quantified ecological metrics. This study implemented a precise, types-to-types alignment between land classes in the CAS ecosystem and the corresponding counterparts within the model's land structural schema, enabling the seamless transference of ecological indicators from the model to the CAS classification system. These indicators were then recalibrated to mirror the distinct ecological dynamics of Heilongjiang region. Also, the proportional weights for subcategories of construction land such as ISA, forest, grassland, BS were added to improve the simulation accuracy of ecosystem services.

Ecological Values for the Different Types of Lands and the Calculation of Ecosystem Services

The baseline unit of the ecological values for the different types of lands always used the net economic benefit corresponding to the annual grain output per hectare of agricultural land [22]. This quantification approach achieved the monetary expression of the ecological values among the different types for ecosystem services valuation. To accurately reflect the regional ecological characteristics, field investigations were conducted in the Heilongjiang region to determine the main crop types. Then, historical net income data for these crops were systematically collected from authoritative official statistical yearbooks and corresponding research institutes and universities, spanning the period from 1970 to 2020. Meanwhile, to avoid inflationary effects over a 50-year period, all monetary values were adjusted for inflation using the 50-year average as the baseline to ensure temporal comparability. Subsequently, the monetary equivalents of ecosystem service factors for different land types were computed in accordance with Formula (1), using the mathematical and statistical methodologies. The ecological values table for the different types of lands in the Heilongjiang region is presented below (Table 1). Then, in 1970, the area of cultivated land was 12,722,171.12 ha, it increased to 17,366,512.18 ha in 2020. Under the driving force of cropland change, the alterations in other land uses were induced, which directed the trajectory of changing direction in ecosystem services using Table 1.

$$E_a = \frac{1}{7}\sum_{i=1}^{n}\frac{m_i p_i q_i}{M} \quad (1)$$

where E*a* was monetary value (yuan/ha); *i* was agricultural crop types of the study area; *M* was total planting area during the period of study (ha); m_i was the cultivated area of agricultural crop i; p_i was price of agricultural crop i (Yuan/ton); and q_i was the yield of the crop.

Table 1. The ecological values for the different land types in the Heilongjiang region (unit: Yuan/ha).

First-Lands	Second-Lands	Culture	Supply			Support			Regulation			
		AL	FP	MP	WRS	SC	MNC	BD	GR	CR	PE	HR
Cultivated land	Paddy land	152.86	2309.91	152.86	−4466.95	16.98	322.71	356.68	1885.29	968.12	288.74	4619.81
	Rain-fed farmland	101.91	1443.69	679.38	33.97	1749.41	203.82	220.80	1137.97	611.45	169.85	458.58
Forest	Woodland	1715.44	458.58	1070.03	560.49	4280.12	322.71	3906.46	3515.81	10,530.45	3057.23	6556.06
	Shrub forest	1171.94	322.71	730.34	373.66	2921.35	220.80	2666.58	2394.83	7184.49	2174.03	5689.84
	Wood forest	1256.86	339.69	781.29	407.63	3159.14	237.78	2887.38	2598.64	7761.96	2309.91	5078.40
	Other forests	1579.57	424.62	985.11	509.54	3940.43	305.72	3600.74	3244.06	9698.21	2836.43	6352.24
Grassland	High, medium coverages	1002.09	390.65	577.48	322.71	2496.74	186.83	2275.94	2055.14	5418.09	1783.38	3974.40
	Low-coverage	764.31	305.72	441.60	237.78	1885.29	152.86	1715.44	1545.60	4059.32	1392.74	2989.29
Water	Streams and rivers, lakes, others	3210.09	1358.77	390.65	14,080.23	1579.57	118.89	4331.07	1307.81	3889.47	9426.45	173,650.55
	Snow	152.86	0.00	0.00	3668.67	0.00	0.00	16.98	305.72	917.17	271.75	12,110.02
Wetland	Wetland	8033.72	866.21	849.23	4399.01	3923.44	305.72	13,366.88	3227.07	6114.46	6114.46	41,153.69
Construction land	Urban–rural settlements, others	299.40	91.40	182.79	97.70	746.92	56.73	680.74	614.55	1723.90	583.04	1197.59
Other lands	Sandy land, gobi, others	101.91	16.98	50.95	33.97	254.77	16.98	237.78	220.80	169.85	696.37	407.63

Abbreviations: Aesthetic landscape (AL), food production (FP), material production (MP), water resources supply (WRS), soil conservation (SC), maintain nutrient circulation (MNC), biological diversity (BD), hydrologic regulation (HR), climate regulation (CR), purify environment (PE), gas regulation (GR).

After obtaining the ecological values for the different types of lands, the ecosystem services were measured according to the Formula (2).

$$ESV = \sum A_i \times VC_i \quad (2)$$

where the ESV was the abbreviation of ecosystem service value, A_i was the area of land type i, and VC_i was the corresponding coefficient value of land type i.

2.4.4. Classification of Ecosystem Service Levels

To provide a clearer description of how cultivated land evolution influences ecosystem service dynamics and to capture the gradations, spatial patterns of ecosystem capacity were categorized into five hierarchical tiers, namely the low-service zone (Level I), moderately low-service zone (Level II), intermediate-service zone (Level III), moderately high-service zone (Level IV), and high-service zone (Level V).

3. Results

3.1. Analysis of Spatiotemporal Characteristics and Their Regional Differences in Cultivated Land Reclamation Levels

3.1.1. Spatiotemporal Characteristics of Changes in Cultivated Land Reclamation Rate at the Different Stages from 1970 to 2020

In 1970, cultivated land in the study area spanned 127,221.71 km^2, representing a reclamation rate of 28.12%. By 2020, this area had grown by 46,443.41 km^2, reaching 173,665.12 km^2, with the cumulative reclamation rate increasing by 10.27% through successive decades of expansion. The area changed by +14,596.10 km^2 in 1970–1980, +11,533.82 km^2 in 1980–1990, +6705.83 km^2 in 1990–2000, +12,959.55 km^2 in 2000–2010, and +648.10 km^2 in 2010–2020. Meanwhile, by comparing the increases in cultivated land area at different time periods between 1970 and 2020, the cultivated land experienced a phase of rapid expansion, characterized by substantial incremental gains across successive decades,

followed by a deceleration in growth during the final decade (i.e., 2010–2020), during which the reclamation rate increased by merely 0.14%, indicating that the era of large-scale agricultural land reclamation had effectively reached its asymptotic limit by 2020.

Spatially, the distribution pattern of cultivated land showed obvious clustering characteristics in 1970, which were mainly located in the southeast, southwest, and northeast regions of the study area (Figure 4); and the cultivated land in other regions was sporadically distributed. Through investigation, we found that these areas with concentrated cultivated land have relatively flat terrain, which was conducive to agricultural cultivation. At the same time, the water network was relatively dense, which was convenient for agricultural irrigation. In the following 50 years (i.e., from 1970 to 2020), the cultivated land expanded in a scattered manner into surrounding land types, with the original planting area in 1970 as the center. Therefore, the concentrated agricultural regions were from 1970. Through monitoring, the key expansions were concentrated in two regions, including central–northern parts and the eastern part in 2020. Especially, the eastern region was suitable for large-scale expansion of agricultural land with fertile soil, dense river networks, and flat terrain.

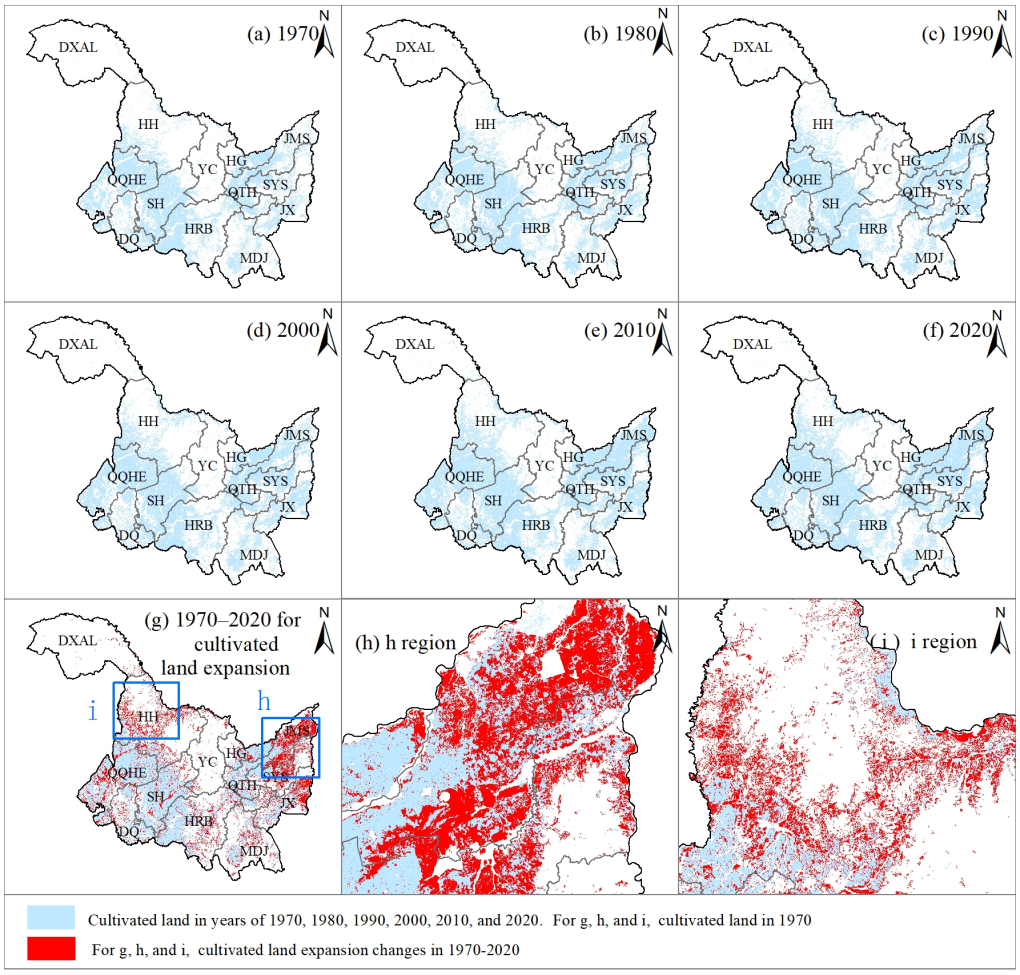

Figure 4. Spatial distribution of cultivated land at a 10-year interval from 1970 to 2020 in the sub-figures (**a**–**f**), and their dynamic changes from 1970 to 2020 for sub-figures (**g**–**i**). Abbreviations: SH: Suihua, SYS: Shuangyashan, QQHE: Qiqihaer, DQ: Daqing, DXAL: Daxinganling, HRB: Haerbin, HG: Hegang, HH: Heihe, JMS: Jiamusi, MDJ: mudanjiang, QTH: Qitaihe, YC: Yichun, and JX: Jixi.

3.1.2. The Differentiated Changes in Cultivated Land Reclamation Level at the City-Scale

Based on land-use data spanning 1970 to 2020 at decadal intervals, the city-level reclamation rate was determined by the proportion of cultivated area relative to the corresponding city's total area. Table 2 displays the results. In 1970, cultivated land reclamation rates exhibited marked regional heterogeneity, with two cities below 10%, two exceeding 50%, and the remaining nine falling within the 10–40% range. Over the 50-year study period, the cultivated land reclamation rates across cities varied from 0.71% to 29.62%, with the maximum value being 4155.29 times than that of the minimum, confirming obvious inter-regional disparities in agricultural land changes. Especially, only Daxinganling had a growth rate of less than 1%. Five cities, Yichun, Mudanjiang, Suihua, Daqing and Haerbin, displayed the changing rate of 3–10%. And another four cities, including Qitaihe, Qiqihaer, Heihe and Jixi, were between 10% and 20%. The top two cities were Chuangyashan and Jiamusi, with changing values of nearly 30%. In 2020, two cities maintained cultivation rates below 10%, while the number exceeding 50% rose from two to four. At the same time, compared to zero cities with reclamation rates of 40–50% in 1970, there were five cities that reached this range in 2020.

Table 2. Statistics of the reclamation rates in 1970, 1980, 1990, 2000, 2010, and 2020, and the corresponding reclamation rate change from 1970 to 2020 (unit: %).

City Names	1970	1980	1990	2000	2010	2020	1970–2020
Daxinganling	0.74	0.94	0.88	1.07	1.26	1.45	0.71
Yichun	5.60	6.60	7.96	8.93	8.72	8.70	3.10
Heihe	14.99	17.83	21.37	24.12	28.88	29.03	14.04
Mudanjiang	19.91	23.05	23.35	24.99	23.72	23.64	3.73
Jixi	29.03	36.58	44.03	46.30	48.44	48.90	19.86
Shuangyashan	31.46	44.38	48.23	51.60	54.40	54.56	23.11
Qitaihe	34.94	39.41	40.59	47.58	46.94	46.69	11.75
Daqing	35.37	36.13	39.88	40.28	42.22	42.73	7.37
Hegang	37.09	39.54	44.00	44.59	44.97	45.10	8.01
Jiamusi	37.10	46.00	50.30	52.04	66.07	66.72	29.62
Haerbin	39.46	41.39	43.57	44.56	47.50	47.40	7.95
Suihua	57.71	59.03	59.19	59.87	63.29	63.28	5.57
Qiqihaer	60.24	63.32	68.02	69.46	72.70	72.82	12.58

3.2. Analysis of the Changing Trend and Differences in the Internal Structure of Cultivated Land

3.2.1. The Evolved Characteristics of the Internal Structure of Cultivated Land

Although cultivated land showed a continuous increase throughout the entire research period, its internal structure types exhibited different trends (Figure 5). In the initial year of the study, rain-fed farmland constituted 25.29% of the study area, while paddy field cultivation remained negligible at 2.83%, reflecting a stark disparity in land-use intensity between the two systems. Then, from 1970 to 2010, both the rain-fed farmland and paddy fields displayed a synchronous growth trend. Specifically, the changing areas of paddy fields were +1694.16 km^2, +1083.92 km^2, +6367.76 km^2, and +12,572.46 km^2 at the studied years, respectively, implying an accelerating trend of the expanding paddy fields. This resulted in the cultivation level of paddy fields being 3.20%, 3.44%, 4.85%, and 7.63% at each year node. Meanwhile, for the rain-fed farmland, although its area continued to increase during 1970–2010, the growth rate gradually decreased, with changing areas of 12,901.95 km^2, 10,449.90 km^2, 338.07 km^2, and 387.09 km^2 at the studied years, respectively. Based on this cultivated speed, the cultivation rates at each year node were 25.29%, 28.15%, 30.46%, 30.53%, and 30.62%. After the year of 2010, different trends were observed, namely, an increase of 9758.06 km^2 in paddy fields promoted the cultivation level to 9.78%; on

the contrary, the reduction in rain-fed farmland area by 9109.95 km^2 led to a decrease in its cultivation rate to 28.60%. For the cultivated land itself, over the 50-year period, the proportional composition of cultivated land shifted significantly, with paddy field share rising steadily from 10.05% in 1970 to 25.49% in 2020. On the contrary, rain-fed farmland declined correspondingly from 89.95% to 74.51%, peaking in 1970.

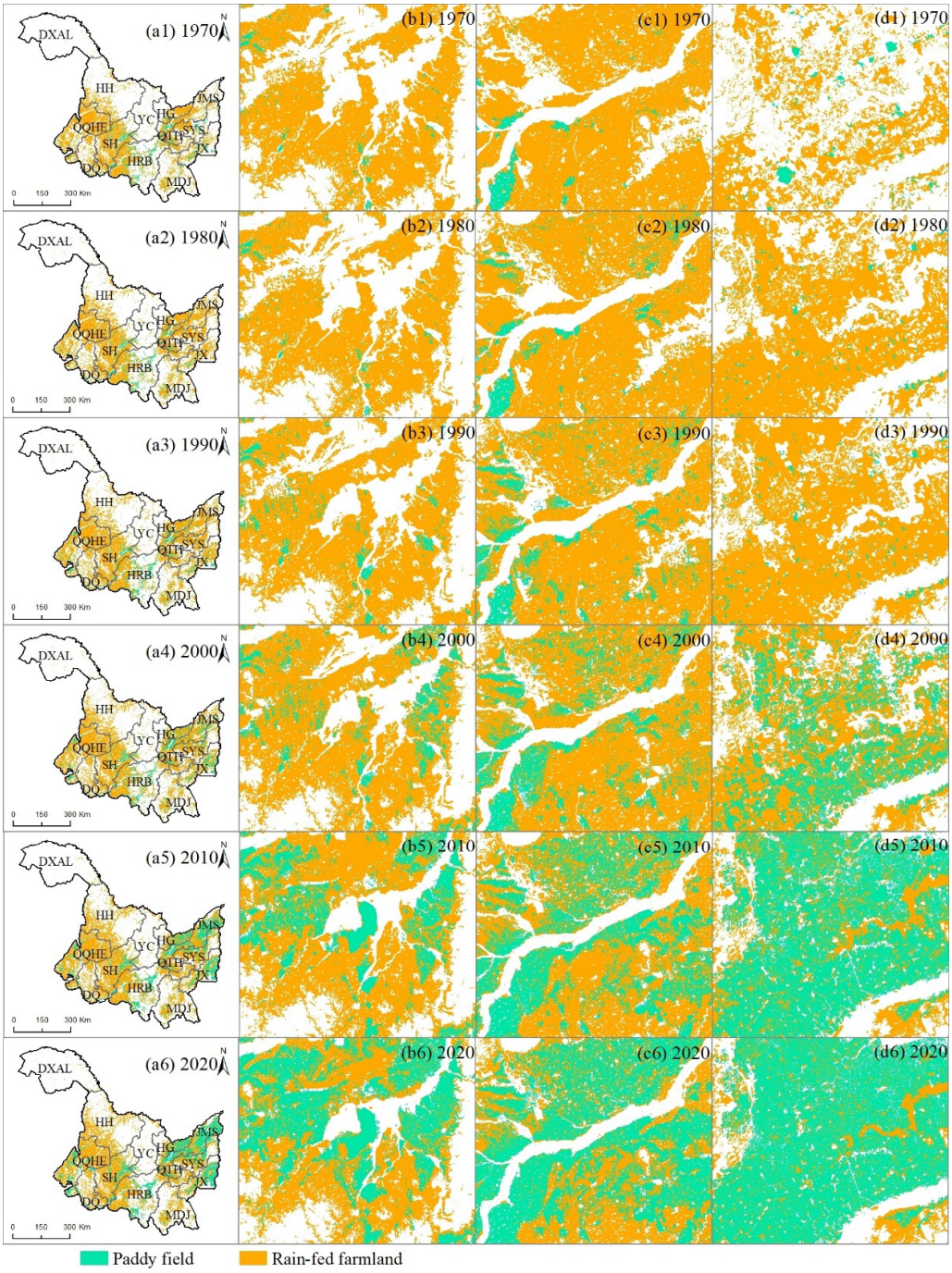

Figure 5. Spatial evolution characteristics of paddy fields and rain-fed farmland. Note: (**a1**–**a6**) are the cultivated land maps for 1970, 1980, 1990, 2000, 2010, and 2020, respectively; (**b1**–**b6**,**c1**–**c6**,**d1**–**d6**) are the enlarged obvious change regions. Abbreviations: SH: Suihua, SYS: Shuangyashan, QQHE: Qiqihaer, DQ: Daqing, DXAL: Daxinganling, HRB: Haerbin, HG: Hegang, HH: Heihe, JMS: Jiamusi, MDJ: mudanjiang, QTH: Qitaihe, YC: Yichun, and JX: Jixi.

3.2.2. Comparison of the Differences in Cultivation Levels Within the Internal Structure of Cultivated Land in Different Cities

Utilizing the secondary land types from 1970 to 2020 and city administrative boundaries, a more granular comparison of cultivation levels between paddy fields and rain-fed farmland was conducted at the city-scale, enabling a deeper investigation into the dynamics of cultivated land structure (Tables 3 and 4). There were obvious differences in the level of cultivation in cultivated land components in different cities. For paddy fields, in the initial year of research, the level of paddy field cultivation in all cities was relatively low, with 10 cities having less than 5% and the other 3 cities ranging from 5% to 10%. Over the next 50 years, the differences in paddy field cultivation rates were monitored. Specifically, Mudanjiang was the only city with a reduced cultivation rate of −0.2%. The increases in Daxinganling, Heihe and Yichun were all less than 1. Forest conservation areas, uneven terrain, and relatively cold climate limited the development of paddy fields in these four cities. Daqing, Qitaihe, Suihua, and Haerbin displayed that the cultivation rate of paddy fields increased by between 3% and 5%. Through investigation, the development of paddy fields in these three cities was primarily constrained by terrain and water resources. Qiqihaer, Chuangyashan, Jiamusi, Hegang, and Jiamusi showed a faster process of paddy field cultivation with values of 9.91–32.33%, in which the fastest paddy field cultivation appeared in Jiamusi. The dense river network, flat terrain, suitable policies and engineering have jointly promoted the rapid development of paddy field cultivation in these five cities.

Table 3. Statistics of the reclamation rates of paddy fields and rain-fed farmland in different cities in 1970, 1980, 1990, 2000, 2010, and 2020, and the corresponding reclamation rate change from 1970 to 2020 (unit: %).

Type	City	1970	1980	1990	2000	2010	2020	1970–2020
Rain-fed farmland	Daxinganling	0.74	0.94	0.88	1.07	1.25	1.44	0.71
	Heihe	14.92	17.82	21.34	24.06	28.7	28.74	13.82
	Yichun	4.43	5.51	6.85	7.8	7.26	6.86	2.43
	Daqing	34.05	34.35	37.7	38.2	39.21	37.58	3.53
	Qiqihaer	58.83	61.59	63.57	64.58	65.85	61.5	2.67
	Hegang	35.55	38.37	41.03	31.38	29.37	21.28	−14.27
	Mudanjiang	17.77	20.72	20.87	22.01	21.6	21.52	3.75
	Qitaihe	61.68	68.97	69.86	80.34	81.01	79.48	17.81
	Shuangyashan	27.16	35.62	46.33	38.7	41.24	36.31	9.15
	Jiamusi	32.67	41.81	44.94	44.15	36.5	28.57	−4.1
	Jixi	23.36	29.73	36.29	36.4	24.65	23.2	−0.16
	Suihua	51.3	53.41	53.96	53.12	54.7	52.17	0.87
	Haerbin	31.18	32.02	33.2	33.92	35.89	34.39	3.21
Paddy fields	Daxinganling	0	0	0	0	0.01	0.01	0.01
	Heihe	0.07	0.01	0.02	0.05	0.17	0.28	0.21
	Yichun	1.17	1.09	1.12	1.14	1.45	1.85	0.67
	Daqing	1.32	1.79	2.18	2.07	3.01	5.16	3.84
	Qiqihaer	1.41	1.73	4.45	4.88	6.85	11.33	9.91
	Hegang	1.54	1.18	2.98	13.21	15.6	23.82	22.28
	Mudanjiang	2.14	2.33	2.48	2.98	2.11	2.12	−0.02
	Qitaihe	4.02	5.12	6.46	9.11	7.23	8.3	4.29
	Shuangyashan	4.3	8.76	1.9	12.9	13.16	18.25	13.96
	Jiamusi	4.43	4.2	5.36	7.89	29.58	38.15	33.72
	Jixi	5.67	6.85	7.75	9.9	23.79	25.69	20.02
	Suihua	6.41	5.61	5.23	6.75	8.58	11.11	4.7
	Haerbin	8.28	9.36	10.37	10.63	11.61	13.01	4.73

Table 4. Statistics of the shares of the rain-fed farmlands (%) and paddy fields (%) to the total cultivated areas in the listed cities throughout the studied years (%).

Type	City	1970	1980	1990	2000	2010	2020
Rain-fed farmland	Daxinganling	100	100	100	100	99.59	99.62
	Heihe	99.53	99.96	99.89	99.78	99.4	99.03
	Yichun	79.05	83.43	85.98	87.26	83.34	78.78
	Daqing	96.28	95.05	94.53	94.86	92.87	87.94
	Qiqihaer	97.65	97.26	93.45	92.98	90.57	84.45
	Hegang	95.84	97.03	93.24	70.37	65.31	47.18
	Mudanjiang	89.25	89.91	89.38	88.07	91.09	91.01
	Qitaihe	93.89	93.09	91.54	89.82	91.81	90.54
	Shuangyashan	86.34	80.27	96.06	75	75.8	66.55
	Jiamusi	88.07	90.88	89.35	84.83	55.24	42.82
	Jixi	80.47	81.27	82.41	78.62	50.88	47.46
	Suihua	88.9	90.49	91.17	88.73	86.44	82.44
	Haerbin	79.02	77.37	76.2	76.14	75.56	72.56
Paddy fields	Daxinganling	0	0	0	0	0.41	0.38
	Heihe	0.47	0.04	0.11	0.22	0.6	0.97
	Yichun	20.95	16.57	14.02	12.74	16.66	21.22
	Daqing	3.72	4.95	5.47	5.14	7.13	12.06
	Qiqihaer	2.35	2.74	6.55	7.02	9.43	15.55
	Hegang	4.16	2.97	6.76	29.63	34.69	52.82
	Mudanjiang	10.75	10.09	10.62	11.93	8.91	8.99
	Qitaihe	6.11	6.91	8.46	10.18	8.19	9.46
	Shuangyashan	13.66	19.73	3.94	25	24.2	33.45
	Jiamusi	11.93	9.12	10.65	15.17	44.76	57.18
	Jixi	19.53	18.73	17.59	21.38	49.12	52.54
	Suihua	11.1	9.51	8.83	11.27	13.56	17.56
	Haerbin	20.98	22.63	23.8	23.86	24.44	27.44

For rain-fed farmland, only Daxinganling and Yichun showed lower levels of cultivation, with values of 0.74% and 4.43%. And the other 12 cities showed relatively high cultivation rates. So, in the initial year of the study, rain-fed farmland constituted the predominant form of cultivated land across these cities. Afterwards, each city experienced varying degrees of agricultural land expansion. Also, several cities displayed signs of contraction after expansion. Finally, the cultivation level of three cities decreased, in which Jiamusi and Jixi displayed slight contractions with 4.10% and 0.16%, but Hegang decreased by as much as 14.27%. On the contrary, the cultivation rate of 10 cities increased. The increment of Daxinganling and Suihua was only 0.71% and 0.87%. Yichun, Qiqihaer, Haerbin, Daqing, and Mudanjiang were about 2% or 3%. Shuangyashan, Heihe, and Qitaihe exhibited high expansion, with improved cultivation rates of 9.15%, 13.82%, and 17.81%. Over the study period, cultivated land transformation within cities followed a distinct two-phase pattern: an initial phase of concurrent expansion in both paddy fields and rain-fed farmland, succeeded by a later phase dominated by paddy field expansion alongside concomitant contraction of rain-fed farmland.

3.3. Analysis of the Outflow and Inflow Characteristics of Cultivated Land and Its Internal Structure

Transformation feature analysis elucidated the sources and destinations of cultivated land dynamics (Figure 6). Between 1970 and 2020, the net expansion was driven by inflows (59,271.48 km^2) exceeding outflows (12,827.11 km^2) by a factor of 4.62, with the primary recipients of converted cropland being construction land, forest, and grassland. These land types collectively accounted for 78.49% of total outflows of cultivated land. In here, the predominant conversion pathway of cultivated land over the past five decades involved

its transformation into construction land, accounting for 33.51% of total land-use change, which reflected the substantial encroachment of urban expansion, rural development, and industrial-mining infrastructure on cultivated land. The second most significant land-use conversion pathway involved the transition of cultivated land into forested areas, accounting for 28.26%, which was primarily driven by the Grain-for-Green Program according to regional investigations.

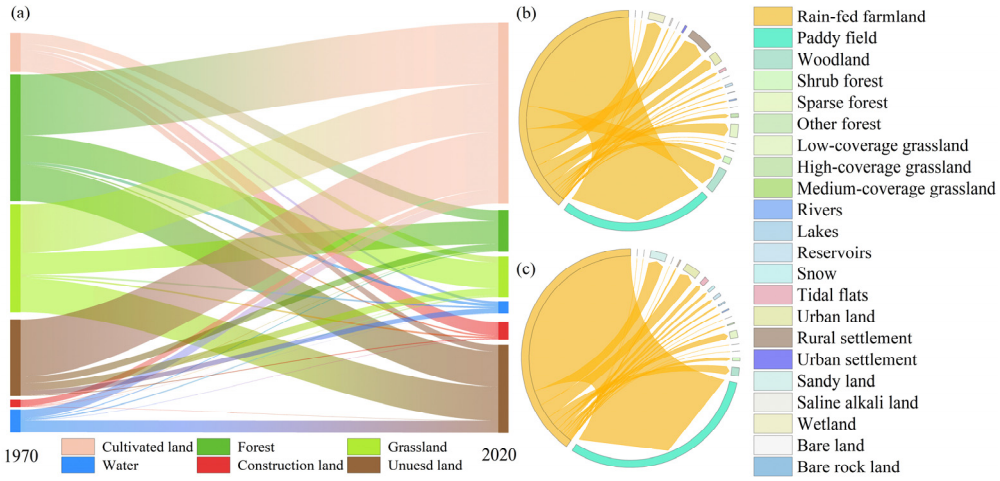

Figure 6. The outflow and inflow characteristics of cultivated land and its internal structure. Note: (**a**) for the first land-level category; (**b**,**c**) for the second land-level category.

Regarding the inflows, the primary inflows to cultivated land were forest and grassland, collectively accounting for 60.41%, predominantly occurring in the agricultural-forestry and agricultural-pastoral ecotones. These areas were adjacent to agricultural land and were convenient for cultivation as farmland. Another important inflow came from unused land, with values of 31.61%. Due to lots of unused land being in a state of no utilization, it was convenient for large-scale cultivation.

Regarding the internal structure of cultivated land, a clear feature displayed that more than half (i.e., 58.34%) of the rain-fed farmland loss has flowed into paddy fields. The transformation within cultivated land dominated the loss of rain-fed farmland. Next was the flow towards construction land and forest, accounting for 13.97% and 12.14%. The proportion of flows to other types was very small. For the inflow of rain-fed farmland, it mainly came from forest, grassland, and unused land, accounting for 39.82%, 26.49%, and 19.21%. Meanwhile, we also found that more than three-quarters (i.e., 75.68%) of paddy fields losses flowed to rain-fed farmland. Through field research and remote sensing image monitoring, we found that many of these lost paddy fields were located in agricultural project areas, some small paddy fields regions were canceled and a large number of concentrated planting areas for rain-fed farmland emerged. From the perspective of inflow, apart from a large amount (46.72%) of rain-fed farmland turning into paddy fields, data monitoring also showed that lots of unused land was converted into paddy fields, accounting for 29.28% of the total inflow of paddy fields, as lots of wetlands, shrubs, etc., were cultivated into paddy fields.

3.4. Analysis of the Characteristics of Changes in Ecosystem Services in the Whole Region

In 1970, the level of urbanization and industrialization in the entire region was relatively low, and many regions were in a state of primitive forest communities, swamps and wetlands, with a high-value ecosystem service of 15,575.87 $\times$ 10^8 yuan (Figure 7). Subsequently, the various factors such as urban construction, rural expansion, industrial and mining development, and agricultural land reclamation led to the loss. Accord-

ing to the results of statistics with a 10-year interval from 1970 to 2020, the values were 14,801.56 × 10^8 yuan, 14,195.44 × 10^8 yuan, 13,869.36 × 10^8 yuan, 13,053.28 × 10^8 yuan, and 12,495.72 × 10^8 yuan in each node. The monitoring data showed that the changes in each time period were −774.31 × 10^8 yuan, −606.12 × 10^8 yuan, −326.09 × 10^8 yuan, −816.07 × 10^8 yuan, and −557.56 × 10^8 yuan, with a total loss of 3080.15 × 10^8 yuan. This value indicated a turnover rate of up to 19.78% over the course of 50 years and an average annual turnover rate of 0.40%. Spatially, for the convenience of clustering display, this study classified the calculated ecosystem service into five levels, including the low-value area (i.e., level I), sub-low value area (i.e., level II), median-value area (i.e., level III), sub-high-value area (i.e., level IV), and high-value area (i.e., level V) (Figure 8). The high-value ecosystem service regions (i.e., level V) were mainly located in the mountains of Daxinganling, Xianxinganling, and Changbai (Figure 8); on the contrary, the low-value ecosystem service regions (i.e., level I) were concentrated in the Songnen Plain and Sanjiang Plain, which were the key regions affected by severe expansion of cultivated land leading to ecosystem decline from 1970 to 2020.

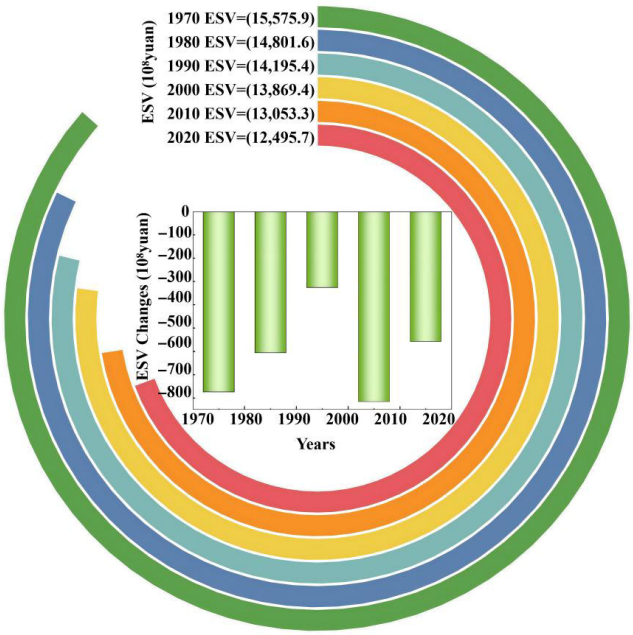

Figure 7. The current status and dynamic statistics of ecosystem services at 10-year intervals.

3.5. Analysis of the Impact of Cultivated Land Changes on Ecosystem Services

3.5.1. Quantitative Analysis of the Impact on Ecosystem Services

Cultivated land expansion was primary land change, which consistently diminished ecosystem services due to its inherently lower ecological carrying capacity. From 1970 to 2020, this expansion induced ecological losses amounting to 529.18 × 10^8 yuan for forest, 148.79 × 10^8 yuan for grassland, 579.58 × 10^8 yuan for water, and 1499.22 × 10^8 yuan for wetland. The data showed that wetland experienced the most loss, followed by water, forest and grassland. In the forest, wooded land had the highest loss of 412.39 × 10^8 yuan, accounting for the proportion of 77.93%, but the loss of shrubs, sparse forest and other forests were only 91.73 × 10^8 yuan, 23.63 × 10^8 yuan, and 1.43 × 10^8 yuan. For grassland, according to the statistics of the data, the proportion of ecological loss between low-coverage grassland, and medium- and high-coverage grasslands was 4.64:1. So, the expansion of cultivated land mainly encroached on low coverage-grassland, and the loss of grassland with medium- and high-coverage were very limited. Meanwhile, considering

the construction land and other land with very small ecological variables, the loss caused by cultivated land expansion over the past 50 years was as high as 2754.08 × 10^8 yuan.

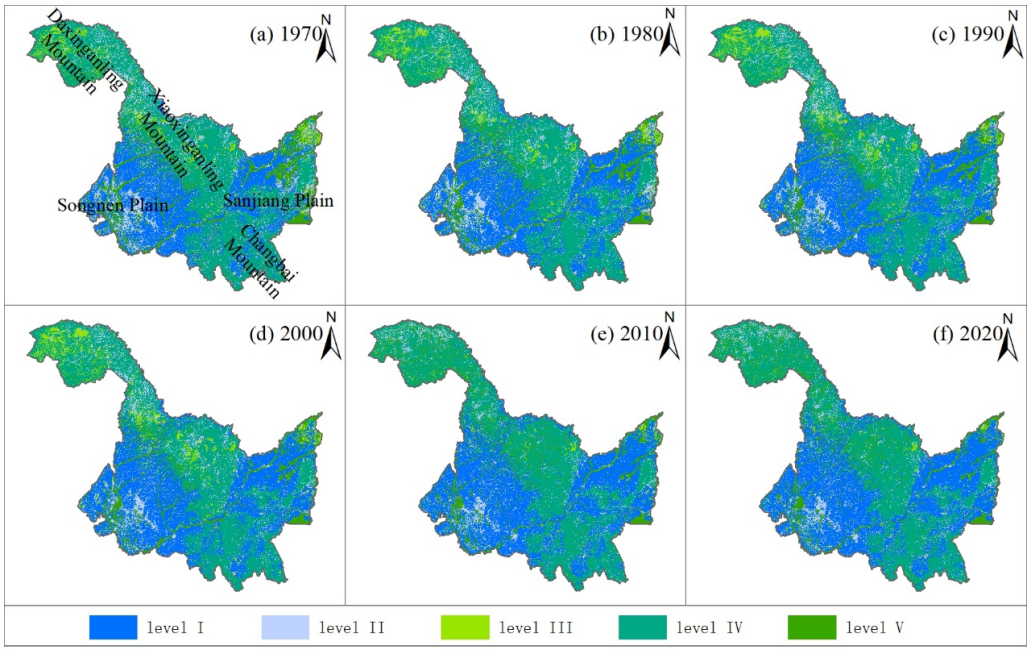

Figure 8. Spatial distribution of ecosystem services from 1970 to 2020. Note: level I: low-value area, level II: sub-low value area, level III: median-value area, level IV: sub-high-value area, and level V: high-value area.

Cultivated land also experienced the shrinkage, and its loss led to an overall improvement of 450.61 × 10^8 yuan in ecosystem services from 1970 to 2020. Specifically, forest and grassland planning, and the returning farmland to forest/grassland promoted the improvement of ecosystem service for 116.37 × 10^8 yuan. The policies such as returning abandoned cultivated land to wetlands increased 162.84 × 10^8 yuan. The occupation by agricultural water conservancy projects, agricultural water diversion irrigation projects, etc., promoted the transformation of cultivated land to water and increased the ecological value by 174.32 × 10^8 yuan. Meanwhile, although a large amount of cultivated land has been transformed into urban, rural, industrial and mining lands, the changes in ecosystem services were relatively weak.

The expansion and shrinkage of cultivated land have led to changes in ecosystem services, with quantities of −2754.08 × 10^8 yuan and +450.61 × 10^8 yuan. This calculation indicated that the net variables were −2303.46 × 10^8 yuan with an average annual change of −46.07 × 10^8 yuan/yr. By comparing the ecological loss of the entire region and cultivated land changes, a phenomenon was found where a three-quarters (i.e., 74.78%) loss was caused by cultivated land change.

3.5.2. The Impact of the Evolution of Paddy Fields and Rain-Fed Farmland on Ecosystem Services

Evolution of cultivated land components has different changes in their impact on the ecosystem. Through the comprehensive statistics, the ecosystem service loss caused by the expansion of paddy fields and the increase caused by the reduction in paddy fields were 1200.19 × 10^8 yuan and 50.97 × 10^8 yuan, with a net loss of +1149.23 × 10^8 yuan from 1970 to 2020. For the expansion of paddy fields, it often led to a decrease in ecosystem service, considering its own lower values. And the loss from paddy fields expansion was mainly concentrated in wetland (847.85 × 10^8 yuan) and water (250.32 × 10^8 yuan), followed by forest (57.89 × 10^8 yuan), grassland (1.13 × 10^8 yuan) and rain-fed farmland

(-3.38×10^8 yuan). The data showed that the extensive transformation of wetland to paddy fields resulted in the highest amount of ecosystem loss. However, another land phenomenon, namely the extensive transformation from rain-fed farmland to paddy fields, only brought small changes, underscoring substantial disparities in the ecological value among land cover types. In the forest, shrub forest incurred the highest ecological loss to paddy fields at 33.25×10^8 yuan, while woodland, sparse forest, and other forest types contributed losses of 16.95×10^8 yuan, 7.58×10^8 yuan, and 0.11×10^8 yuan. Conversely, the ecological decline resulting from paddy field loss was predominantly driven by water (24.85×10^8 yuan) and wetlands (19.87×10^8 yuan), followed by forest (4.61×10^8 yuan), grassland (1.13×10^8 yuan), and rain-fed farmland (0.62×10^8 yuan).

Meanwhile, the expansion of rain-fed farmland resulted in a net reduction in ecosystem services by 1556.65×10^8 yuan, whereas its contraction contributed an increase of 396.89×10^8 yuan. During expansion, ecological losses from other land types amounted to 471.29×10^8 yuan for forest, 107.83×10^8 yuan for grassland, 329.26×10^8 yuan for water, and 651.37×10^8 yuan for wetland. The wetland-to-rain-fed-farmland transition accounted for the highest loss. Among forest types, woodland conversion to rain-fed farmland induced the greatest loss at 395.44×10^8 yuan, followed by shrub forest (58.48×10^8 yuan), sparse forest (16.05×10^8 yuan), and other forests (1.32×10^8 yuan). Conversely, the loss of rain-fed farmland was associated with ecosystem service gains, particularly from water (149.47×10^8 yuan), wetlands (142.98×10^8 yuan), forest (93.16×10^8 yuan), and grassland (17.47×10^8 yuan).

From the perspective of various functions of the ecosystem, the supply service decreased by 13.92%. Further analysis of the data through mathematical statistics indicated that this decreasing trend was due to the significant reduction in regional water resource supply caused by the expansion of paddy fields. In the process of expansion of cultivated land, adjustment service, support service and cultural service increased by 75.37%, 21.13%, 46.54% from 1970 to 2020. Internally within each service, there have also been obviously changes in various indicators, such as the biodiversity increased by nearly 48.72% as well as landscape aesthetics for 46.54%.

4. Discussion

4.1. Important Role of Cultivated Land of Northeast China in the Evolution of National Cultivated Land in the Past 50 Years

In Northeast China, there has been extensive monitoring of cultivated land and its internal changes [30,31]; however, this study was the first to quantitatively explore the evolution of cultivated land and its resulting loss of ecological services in the Heilongjiang region in the past 50 years. According to land change statistics, an important quantitative discovery was that the remote sensing monitoring data displayed that the cultivated land of this study increased by 46,443.41 km^2 from 1970 to 2020 (Figure 4). And a drastic land reorganization within the cultivated land showed that the proportion of rain-fed farmland and paddy field changed from 89.95% vs. 10.05% in 1970 to 74.51% vs. 25.49% in 2020 (Table 2). This was important in area growth and structural adjustment of farmland changes in China. Firstly, for the cultivated land area, as is widely known, China was a large country with a population of over 13 billion people. However, its cultivated land resources only made up about 9% of the global cultivated land area [32]. This indicated that China's average arable land per person fell below the worldwide norm [33]. The scarcity of cultivated land to support a massive population has remained a core national reality in China, enduring from the past through the present and into the foreseeable future [34]. The expansion of cultivated land in Heilongjiang, a key agricultural hub in China [35], played an important role in maintaining the nation's total cultivated land base during

1970–2020, particularly in upholding China's 1.8 billion-acre farmland protection threshold. The preservation of China's cultivated land base confronts multifaceted pressures. The accelerated urban and industrial expansion has precipitated substantial cropland depletion in southeastern coastal zones and metropolitan clusters including the Beijing–Tianjin–Hebei nexus [36,37]. And in the Huabei region of China, the soil deterioration and salinization have compromised land productivity [38]. The arid conditions and insufficient rainfall severely restrict the viability of extensive cereal cultivation across the Inner Mongolian Plateau [39], Qinghai–Tibet Plateau [40] and Northwest China [41,42]. In Northeast China, especially in the Heilongjiang region, the increase in cultivated land was very important for China (Figure 4).

Northeast China accounted for approximately one-quarter of the nation's total grain production [43,44]. Through investigation, it was found that the original planting structure, which was mainly based on rain-fed farmland such as soybeans, corn, sorghum, and millet, has gradually shifted to a parallel planting structure of rain-fed farmland (i.e., corn) and paddy fields (i.e., rice). This change in planting structure deeply reflected the reform of China's grain crops. Before the year 2000, the main purpose of cultivating farmland was ration security and to enable people to reach a level of subsistence (i.e., not starving) [44]. The crops, such as soybeans, corn, sorghum, and millet, were widely planted due to being largely unconstrained by the natural environment. After China's accession to WTO [44], corn became a main crop in rain-fed farmland, while the planting area of soybeans has significantly shrunk. When there was an excess of corn production in China, the national policy of agricultural structural reform was implemented, requiring the optimization of a crop planting structure. In this context, in Northeast China, especially in the Heilongjiang region (Figure 5), a substantial conversion of rain-fed cropland into paddy fields occurred, primarily driven by the prevalence of gently sloping topography, high availability of water, elevated soil organic carbon levels, extensive coverage of black soils, and the widespread presence of state-owned agricultural enterprises.

4.2. The Expansion of Cultivated Land Resulted in a 74.78% Decline in Ecosystem Services Across the Entire Region

The total loss of ecological services was 3080.15×10^8 yuan according to the statistics of ecological changes in the Heilongjiang region from 1970 to 2020. Based on the statistical results of the model, the total amount of ecosystem service loss caused by the evolution of cultivated land was 2303.46×10^8 yuan, which accounted for three-quarters (i.e., 74.78%) (Figure 9). This means that the evolution of cultivated land dominated the changes in ecosystem services throughout the study area. The main reasons for this phenomenon may be as follows. (1) Large-scale loss of native wetlands with high-ecological value. In ancient China, Northeast China, especially the Heilongjiang region, was mostly sparsely populated areas with overgrown weeds and predominantly native natural environments. To meet the demand for food security, these natural wetlands were extensively cultivated as agricultural land in the past century [45], which was characterized by high-organic matter content, flat topography, abundant water supply, and favorable climatic conditions, extensively converting into paddy fields (i.e., artificial wetlands) [29,46,47]. (2) The concentration and large-scale cultivation of cultivated land by lots of state-owned farms. Many agricultural policies and water conservancy projects were prioritized for implementation in these state-owned farms, which promoted land leveling, scaling, centralization, mechanization, and intelligence such as the 'High standard farmland engineering', 'Land Consolidation Project in the Eastern Sanjiang Plain', 'Soil fertility protection and crop rotation' [29,48]. During this process, lots of forest and river with high-ecological values were re-cultivated and planned. Extensive cultivation of cultivated land with low-ecological value was enabled rapid expansion. (3) Constraints of nature reserves and state-owned forest farms [49]. Although

extensive cultivation of farmland has led to ecosystem loss, some natural reserve regions, such as the Honghe wetland reserve, prohibited the cultivation of arable land. There were also lots of state-owned forest farms in Heilongjiang region, such as in Daxing'anling and Xiaoxian'anling mountains [50]. Although the natural environment of these areas can be cultivated as farmlands, the farmland was prohibited due to the need for forest protection. Therefore, in the differences between promotion and prohibition of cultivated land, its expansion led to the loss of three-quarters of the regional ecology.

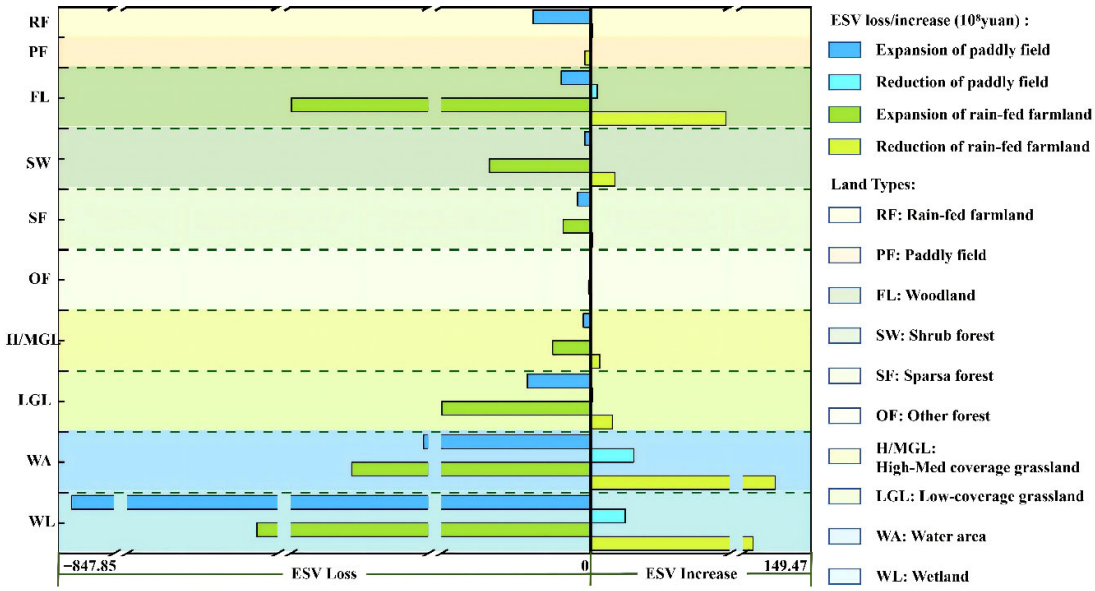

Figure 9. The impact of cultivated land structure evolution on ecosystems.

4.3. Measures and Suggestions for Ecosystem Restoration

Despite extensive losses in regional ecosystem services due to cultivated land expansion in Northeast China from 1970 to 2020 (Figures 7 and 9), the targeted interventions remained the viable to bolster regional ecological security. From the perspectives of policies and projects, China implemented a strategic ecological project called 'the Three-North Shelterbelt Program Project'. This project aimed to prevent wind-sand erosion and improve the ecological environments through forest planting. There were a large number of project regions for this project in the Heilongjiang region. Through the period of the sixth period (2021–2030) in Heilongjiang region [51], the transformation of cultivated land to forest can be accelerated to a certain extent to increase forest land planting and improve ecosystem services. Meanwhile, in some degraded wetland regions, wetland restoration projects should be implemented to restore vegetation cover, enhance water conservation and carbon sequestration capabilities. In agricultural production regions, crop patch protective forests should be planted more [52], accompanied by the drainage systems and irrigation facilities to enhance ecological service functions. And in wetland conservation areas and state-owned forest farms, it should be necessary to continuously strengthen and protect existing wetland and forestry resources to avoid their degradation, to maintain the stability of the existing ecosystems.

4.4. Research Shortcomings and Prospects

Although this study spans a five-decade period from 1970 to 2020, it fails to account for recent land-use transformations, especially those manifesting in 2025. Future efforts will integrate the remote sensing observations with advanced digital classification methodologies to produce high-resolution land cover maps for the year of 2025, thereby facilitating

a more timely and precise evaluation of the environmental consequences associated with land-use dynamics. Further, although this study conducted complex statistics on land-use tracking trajectories, landscape measurement values, and ecosystem service simulation results, a broader linking between complex statistics and conclusions should be further explored and discussed in future research. Meanwhile, the valuation method is primarily based on a market equivalence factor system grounded in grain yield. It may lead to an underestimation of non-material ecological benefits that are difficult to convert into agricultural market value, such as aesthetic experience, spiritual enjoyment, and relaxed mood, which will become the direction of our next research.

5. Conclusions

Focusing on the scientific issue of long-term monitoring of cultivated land and its impact on ecosystem services in the Heilongjiang region of Northeast China, the integrated methods of land update technology, dynamic tracking, remote sensing classification, and the improved ecosystem services were applied. The main conclusions were below.

(1) Through remote sensing satellite monitoring, the area of cultivated land was 127,221.71 km^2, with a reclamation rate of 28.12% in 1970. A continuously increasing trend was monitored, with net changes of 46,443.41 km^2 and a growth rate of 10.27% from 1970 to 2020; the cover reached to 173,665.12 km^2 in 2020. Spatially, the key expansion region was mainly concentrated in central–northern parts and the eastern part.

(2) Regarding the structure, 25.29% of the study area was covered by rain-fed farmland, but only 2.83% for paddy fields in the initial year. Subsequently, an increasing trend was monitored in both land types with 28.60% and 9.78% in the ending year, displaying only a 13.08% increment in rain-fed farmland and 246.14% in paddy fields.

(3) The source area of cultivated land was 59,271.48 km^2, with 60.41% from forest and grassland of the agricultural-forestry ecotone and 31.61% from unused land. Meanwhile, its destination area was 12,827.11 km^2, and 78.49% of the total was construction land, forest, and grassland. By comparison, the source was 4.62 times that of the destination. Within the internal structure, an obvious difference was that most of the paddy fields came from rain-fed farmland (75.68%) and wetland (6.03%), but rain-fed farmland was mainly from forest (39.82%) and grassland (26.49%).

(4) In 1970, the ecosystem service was 15,575.87 $\times$ 10^8 yuan, and the monitoring data showed a continuously decreasing trend, with the 10-year interval changes of -774.31×10^8 yuan, -606.12×10^8 yuan, -326.09×10^8 yuan, -816.07×10^8 yuan, and -557.56×10^8 yuan from 1970 to 2020, a total loss of 3080.15×10^8 yuan and an annual turnover rate of 0.40%.

(5) A phenomenon was found in which three-quarters (i.e., 74.78%) of loss was caused by cultivated land, indicating that the ecosystem services were controlled by cultivated land changes. Another important discovery was that a large transformation of wetlands into paddy fields led to the huge loss of 847.85×10^8 yuan; by contrast, the process of extensive rain-fed farmland turning into paddy fields was only a small change of 3.38×10^8 yuan.

To enhance ecosystem services, the central government should continue the 'Three-North Shelterbelt Program Project' to promote forest restoration. For the local government, the restoration should prioritize vegetation recovery to bolster water retention and carbon sequestration in degraded wetlands, and it also should expand crop patch protective forests integrated with the optimized drainage and irrigation infrastructure in agricultural zones. Farmers could enhance ecosystem services through practices such as crop rotation, replacing chemical fertilizers with organic fertilizers, and substituting chemical pesticides with biological control methods.

Author Contributions: Conceptualization, Z.Y.; methodology, Z.Y.; formal analysis, Z.Y. and T.P.; writing—original draft preparation, Z.Y.; writing—review and editing, T.P., Z.L., L.S., N.Z., H.Z. and B.L. All authors have read and agreed to the published version of the manuscript.

Funding: This work was supported by the National Natural Science Foundation of China (42171126). Tao Pan was funded by the Rizhao Natural Science Foundation (Grant No. RZ2024ZR17).

Data Availability Statement: Data will be made available on request.

Acknowledgments: The authors would like to thank the editor and anonymous reviewers for their helpful and constructive comments to improve this article.

Conflicts of Interest: The authors declare no conflicts of interest.

References

1. Jónsdóttir, S.; Gísladóttir, G. Land use planning, sustainable food production and rural development: A literature analysis. *Geogr. Sustain.* **2023**, *4*, 391–403. [CrossRef]
2. Xu, Z.; Peng, J.; Dong, J.; Liu, Y.; Liu, Q.; Lyu, D.; Qiao, R.; Zhang, Z. Spatial correlation between the changes of ecosystem service supply and demand: An ecological zoning approach. *Landsc. Urban Plan.* **2022**, *217*, 104258. [CrossRef]
3. Martinez-Harms, M.J.; Bryan, B.A.; Figueroa, E.; Pliscoff, P.; Runting, R.K.; Wilson, K.A. Scenarios for land use and ecosystem services under global change. *Ecosyst. Serv.* **2017**, *25*, 56–68. [CrossRef]
4. Mori, A.S.; Gonzalez, A.; Seidl, R.; Reich, P.B.; Dee, L.; Ohashi, H.; Hautier, Y.; Loreau, M.; Isbell, F. Urgent climate action is needed to ensure effectiveness of protected areas for biodiversity benefits. *One Earth* **2024**, *7*, 1874–1885. [CrossRef]
5. Varzakas, T.; Smaoui, S. Global Food Security and Sustainability Issues: The Road to 2030 from Nutrition and Sustainable Healthy Diets to Food Systems Change. *Foods* **2024**, *13*, 306. [CrossRef] [PubMed]
6. Mishenin, Y.; Yarova, I.; Koblianska, I. Ecologically Harmonized Agricultural Management for Global Food Security. In *Ecological Intensification of Natural Resources for Sustainable Agriculture*; Jhariya, M.K., Meena, R.S., Banerjee, A., Eds.; Springer: Singapore, 2021; pp. 29–76.
7. Gozdowski, D.; Žukovskis, J.; Razinkovas-Baziukas, A.; Wójcik-Gront, E. Land Cover Changes in Selected Areas Next to Lagoons Located on the Southern Coast of the Baltic Sea, 1984–2021. *Sustainability* **2022**, *14*, 2006. [CrossRef]
8. Xie, H.; Wang, W.; Zhang, X. Evolutionary game and simulation of management strategies of fallow cultivated land: A case study in Hunan province, China. *Land Use Policy* **2018**, *71*, 86–97. [CrossRef]
9. Yang, G.; Li, S.; Wang, H.; Wang, L. Study on agricultural cultivation development layout based on the matching characteristic of water and land resources in North China Plain. *Agric. Water Manag.* **2022**, *259*, 107272. [CrossRef]
10. Yao, Z.; Zhang, L.; Tang, S.; Li, X.; Hao, T. The basic characteristics and spatial patterns of global cultivated land change since the 1980s. *J. Geogr. Sci.* **2017**, *27*, 771–785. [CrossRef]
11. Liu, J.; Kuang, W.; Zhang, Z.; Xu, X.; Qin, Y.; Ning, J.; Zhou, W.; Zhang, S.; Li, R.; Yan, C. Spatiotemporal characteristics, patterns, and causes of land-use changes in China since the late 1980s. *J. Geogr. Sci.* **2014**, *24*, 195–210. [CrossRef]
12. Sui, J.; Dai, Y. Analysis of conservation practices for black soil based on organic matter and nitrogen contents in the black soil region of Northeast China. *Sci. Rep.* **2025**, *15*, 23989. [CrossRef]
13. Chu, X.; Zhan, J.; Li, Z.; Zhang, F.; Qi, W. Assessment on forest carbon sequestration in the Three-North Shelterbelt Program region, China. *J. Clean. Prod.* **2019**, *215*, 382–389. [CrossRef]
14. Dangayach, R.; Pandey, A.K. Technologies and Methods for Land Use and Land Cover: A Comprehensive Review. In *Remote Sensing and GIS Application in Forest Conservation Planning*; Moharir, K., Pande, C.B., Eds.; Springer Nature: Singapore, 2025; pp. 369–390.
15. Friedl, M.A.; McIver, D.K.; Hodges, J.C.F.; Zhang, X.Y.; Muchoney, D.; Strahler, A.H.; Woodcock, C.E.; Gopal, S.; Schneider, A.; Cooper, A.; et al. Global land cover mapping from MODIS: Algorithms and early results. *Remote Sens. Environ.* **2002**, *83*, 287–302. [CrossRef]
16. Zhu, K.; Lin, D.; Fu, H.; Zhang, T.; Li, D.; Wang, X.; Liu, Y. Accuracy and consistency assessment of forest cover datasets: A comparative study of two provinces in China. *Front. For. Glob. Change* **2025**, *8*, 1627998. [CrossRef]
17. Pan, Y.; Wang, D.; Li, X.; Liu, Y.; Huang, H. Comparison and Evaluation of Five Global Land Cover Products on the Tibetan Plateau. *Land* **2024**, *13*, 522. [CrossRef]
18. Teijido-Murias, I.; Barrio-Anta, M.; López-Sánchez, C.A. Evaluation of Correction Algorithms for Sentinel-2 Images Implemented in Google Earth Engine for Use in Land Cover Classification in Northern Spain. *Forests* **2024**, *15*, 2192. [CrossRef]
19. Ning, J.; Liu, J.; Kuang, W.; Xu, X.; Zhang, S.; Yan, C.; Li, R.; Wu, S.; Hu, Y.; Du, G. Spatiotemporal patterns and characteristics of land-use change in China during 2010–2015. *J. Geogr. Sci.* **2018**, *28*, 547–562. [CrossRef]

20. Wang, B.; Zhang, Q.; Cui, F. Scientific research on ecosystem services and human well-being: A bibliometric analysis. *Ecol. Indic.* **2021**, *125*, 107449. [CrossRef]
21. Costanza, R. Social Goals and the Valuation of Ecosystem Services. *Ecosystems* **2000**, *3*, 4–10. [CrossRef]
22. Xie, G.; Zhang, C.; Zhen, L.; Zhang, L. Dynamic changes in the value of China's ecosystem services. *Ecosyst. Serv.* **2017**, *26*, 146–154. [CrossRef]
23. Chen, K.; Wang, Y.; Huang, C.; Wang, J.; Li, S.L.; Guan, H.; Ma, L. GreenNet: A dual-encoder network for urban green space classification using high-resolution remotely sensed images. *Int. J. Appl. Earth Obs. Geoinf.* **2025**, *142*, 104709. [CrossRef]
24. Cruz, C.; Perrin, P.M.; Martin, J.R.; O'Connell, J.; McGuinness, K.; Connolly, J. Mapping of temperate upland habitats using high-resolution satellite imagery and machine learning. *Environ. Monit. Assess.* **2024**, *196*, 869. [CrossRef] [PubMed]
25. Jiang, L.; Wang, Z.; Zuo, Q.; Du, H. Simulating the impact of land use change on ecosystem services in agricultural production areas with multiple scenarios considering ecosystem service richness. *J. Clean. Prod.* **2023**, *397*, 136485. [CrossRef]
26. Liu, Y.; Liu, X.; Liu, Z. Effects of climate change on paddy expansion and potential adaption strategies for sustainable agriculture development across Northeast China. *Appl. Geogr.* **2022**, *141*, 102667. [CrossRef]
27. Wang, B.; Tian, J.; Wang, S. Process and mechanism of transition in regional land use function guided by policy: A case study from Northeast China. *Ecol. Indic.* **2022**, *144*, 109527. [CrossRef]
28. Xi, Z.; Chen, G.; Xing, Y.; Xu, H.; Tian, Z.; Ma, Y.; Cui, J.; Li, D. Spatial and temporal variation of vegetation NPP and analysis of influencing factors in Heilongjiang Province, China. *Ecol. Indic.* **2023**, *154*, 110798. [CrossRef]
29. Qian, J.; Zhao, H.; Wang, X.; Wang, T.; Feng, Z.; Cao, C.; Li, X.; Zhang, A. Declining suitability for conversion of drylands to paddy fields in Northeast China: Impact of future climate and socio-economic changes. *Geogr. Sustain.* **2025**, *6*, 100199. [CrossRef]
30. Gao, J.; Zhu, Y.; Zhao, R.; Sui, H. The Use of Cultivated Land for Multiple Functions in Major Grain-Producing Areas in Northeast China: Spatial-Temporal Pattern and Driving Forces. *Land* **2022**, *11*, 1476. [CrossRef]
31. Miao, X.; Li, Z.; Wang, M.; Mei, J.; Chen, J. Measurement of cultivated land ecosystem resilience in black soil region of Northeast China under the background of cultivated land protection policy in China: Case study of Qiqihar City. *J. Clean. Prod.* **2024**, *434*, 140141. [CrossRef]
32. Zhou, Y.; Li, X.; Liu, Y. Cultivated land protection and rational use in China. *Land Use Policy* **2021**, *106*, 105454. [CrossRef]
33. Hu, Y.; Li, B.; Zhang, Z.; Wang, J. Farm size and agricultural technology progress: Evidence from China. *J. Rural Stud.* **2022**, *93*, 417–429. [CrossRef]
34. Fei, L.; Shuang, M.; Xiaolin, L. Changing multi-scale spatiotemporal patterns in food security risk in China. *J. Clean. Prod.* **2023**, *384*, 135618. [CrossRef]
35. Li, X.; Wu, K.; Yang, Q.; Hao, S.; Feng, Z.; Ma, J. Quantitative assessment of cultivated land use intensity in Heilongjiang Province, China, 2001–2015. *Land Use Policy* **2023**, *125*, 106505. [CrossRef]
36. Lin, L.; Ge, E.; Liu, X.; Liao, W.; Luo, M. Urbanization effects on heat waves in Fujian Province, Southeast China. *Atmos. Res.* **2018**, *210*, 123–132. [CrossRef]
37. Zhang, F.; Xu, N.; Wang, C.; Guo, M.; Kumar, P. Multi-scale coupling analysis of urbanization and ecosystem services supply-demand budget in the Beijing-Tianjin-Hebei region, China. *J. Geogr. Sci.* **2023**, *33*, 340–356. [CrossRef]
38. Zhou, S.; Gao, Y.; Zhang, J.; Pang, J.; Hamani, A.K.M.; Xu, C.; Dang, H.; Cao, C.; Wang, G.; Sun, J. Impacts of Saline Water Irrigation on Soil Respiration from Cotton Fields in the North China Plain. *Agronomy* **2023**, *13*, 1197. [CrossRef]
39. Wang, C.; Li, L.; Yan, Y.; Cai, Y.; Xu, D.; Wang, X.; Chen, J.; Xin, X. Effects of cultivation and agricultural abandonment on soil carbon, nitrogen and phosphorus in a meadow steppe in eastern Inner Mongolia. *Agric. Ecosyst. Environ.* **2021**, *309*, 107284. [CrossRef]
40. Huang, J.; Xie, Y.; Chen, L.; Gao, P. Exploring the sustainable land-use planning for Qinghai in the third pole: Scenario-based trade-offs. *Ecol. Front.* **2025**, *45*, 1097–1106. [CrossRef]
41. Xv, Z.; Lv, A. Spatiotemporal dynamics of cultivated land and its impact on water security in northern China. *Agric. Water Manag.* **2025**, *318*, 109744. [CrossRef]
42. Li, D.; Xu, E.; Zhang, H. Influence of ecological land change on wind erosion prevention service in arid area of northwest China from 1990 to 2015. *Ecol. Indic.* **2020**, *117*, 106686. [CrossRef]
43. Cao, X.; Wu, N.; Adamowski, J.; Wu, M. Assessing the contribution of China's grain production during 2005–2020 from the perspective of the crop-water-land nexus. *J. Hydrol.* **2023**, *626*, 130376. [CrossRef]
44. Liang, X.; Jin, X.; Han, B.; Sun, R.; Xu, W.; Li, H.; He, J.; Li, J. China's food security situation and key questions in the new era: A perspective of farmland protection. *J. Geogr. Sci.* **2022**, *32*, 1001–1019. [CrossRef]
45. Tian, A.; Xu, T.; Gao, J.; Liu, C.; Han, L. Multi-scale spatiotemporal wetland loss and its critical influencing factors in China determined using innovative grid-based GWR. *Ecol. Indic.* **2023**, *149*, 110144. [CrossRef]
46. Li, Z.; Liu, M.; Hu, Y.; Xue, Z.; Sui, J. The spatiotemporal changes of marshland and the driving forces in the Sanjiang Plain, Northeast China from 1980 to 2016. *Ecol. Process.* **2020**, *9*, 24. [CrossRef]

47. Luo, C.; Liu, H.-j.; Fu, Q.; Guan, H.-x.; Ye, Q.; Zhang, X.-l.; Kong, F.-c. Mapping the fallowed area of paddy fields on Sanjiang Plain of Northeast China to assist water security assessments. *J. Integr. Agric.* **2020**, *19*, 1885–1896. [CrossRef]
48. Qi, Y.; Hou, Y.; Li, Y.; Li, L.; Zhang, J.; Chang, Y.; Zhu, D. The price gap between state-owned and collective farmlands: Evidence from Xinjiang and Heilongjiang, China. *Land Use Policy* **2023**, *124*, 106460. [CrossRef]
49. Liang, C.; Wei, X.; Meng, J.; Chen, W. How to Improve Forest Carbon Sequestration Output Performance: An Evidence from State-Owned Forest Farms in China. *Forests* **2022**, *13*, 778. [CrossRef]
50. Wu, S.; Shi, S.; Zhang, J. Evolution Analysis of Ecological Security Pattern in Forest Areas Coupling Carbon Storage and Landscape Connectivity: A Case Study of the Xiaoxing'an Mountains, China. *Forests* **2025**, *16*, 331. [CrossRef]
51. Guan, X.; Wang, S.; Xu, M.; Ji, J.; Cao, C. Long-term ecological effectiveness of the Three-North shelterbelt program assessed by changes in ecosystem services. *Sci. Rep.* **2026**, *16*, 8330. [CrossRef]
52. Oon, A.; Ahmad, A.; Md Sah, S.; Abdul Maulud, K.N.; Yahya, M.S.; Lechner, A.M.; Azhar, B. The conservation of biodiverse continuous forests and patches may provide services that support oil palm yield: Evidence from satellite crop monitoring. *Clean. Prod. Lett.* **2023**, *4*, 100036. [CrossRef]

Disclaimer/Publisher's Note: The statements, opinions and data contained in all publications are solely those of the individual author(s) and contributor(s) and not of MDPI and/or the editor(s). MDPI and/or the editor(s) disclaim responsibility for any injury to people or property resulting from any ideas, methods, instructions or products referred to in the content.